

OPEN

Initial pyrolysis mechanism and product formation of cellulose: An Experimental and Density functional theory(DFT) study

Qing Wang*, Hao Song, Shuo Pan, Nanhang Dong, Xinmin Wang & Shipeng Sun

In this paper, analytical pyrolyzer coupled with a gas chromatography–mass spectrometry set-up (Py-GC/MS) and density functional theory(DFT) theory was used to reveal the initial pyrolysis mechanism and product formation mechanism of cellulose pyrolysis. We demonstrated an experimentally benchmarked molecular simulation approach that delineates pyrolysis process of cellulose.

Experimental results indicated that the cellulose pyrolysis products mostly incorporate levoglucosan (LG), glycolaldehyde (HAA), 5-hydroxyfurfural (5-HMF), and the like. The constituents of fast pyrolysis products of cellulose and cellobiose demonstrated the identical trend, although the contents of certain products are different. Laying the foundation of experimental analysis, the reaction pathways of four categories of cellulose pyrolysis were outlined using DFT theory; the pathways are those of generating LG, HAA, and 5-HMF and the dehydration reaction in the process of cellulose pyrolysis. Also, by comparing the energy barriers of various reactions, the optimal pathway of different reactions were summarized. The deduced cellulose pyrolysis reaction pathway opened up new ideas for studying the pyrolysis behavior of cellulose.

Biomass is a clean renewable fuel source, and energy from biomass will definitely play a significant role in new energy systems in the future¹. Pyrolysis is an important method of thermochemical conversion, which converts biomass into bio-oil and has the advantages of easy storage, transportation and high energy density. Therefore, biomass pyrolysis technology is considered to be a promising approach to the use of biomass energy. Biomass is a complex material that is mainly composed of crosslinked hemicellulose, cellulose, and lignin, along with extracts (tannins, fatty acids, and resins) and inorganic salts². Numerous studies have indicated that cellulose is the most abundant organic linear polymer³. It is composed of D-glucose as a basic unit and is linked via β -O-4 glycosidic bonds. First, there are two controversial perspectives with respect to cellulose crystallinity. One contends that cellulose has a strong crystal structure^{4,5}, whereas the other⁶ insists that cellulose has both crystalline and amorphous regions, depending on the periodic or random distribution of microfibrils in the cellulose. Second, Each glucose monomer has six carbon atoms, two of which are attached to the glycosidic bond, and the other four are each attached to a hydroxyl group⁷. Previous research stated briefly that there are more active hydrogen bonds on glucopyranose⁸. These are some of the main features of cellulose. Because cellulose is the main component of biomass, studying the pyrolysis mechanism of cellulose contributes to understanding the pyrolysis law of biomass, which lays a foundation for developing the biomass pyrolysis process and the effective utilization of energy from biomass.

In depth studying the pyrolysis mechanism of cellulose is crucial to further understanding the thermochemical transformation of biomass. Previously, researchers proposed multifarious reaction kinetic models. Broido and Shafizadeh put forward the “B-S” model and proposed the theory that cellulose depolymerizes via heat to form active cellulose and that two kinds of parallel reactions occur. The earliest reaction has been recognized to be authoritative. Bradbury⁹ *et al.* considered that cellulose macromolecules undergo intermediate physical and chemical changes, such as vitrification¹⁰ or depolymerization¹¹ to degree of polymerization(DP) approximate 200, and then it is transformed into designated products. This is in line with the B-S model and has been studied in more depth. Previous studies on cellulose pyrolysis have reported that the chemical and physical details of the

Engineering Research Centre of Oil Shale Comprehensive Utilization, Ministry of Education, Northeast Electric Power University, Jilin City, Jilin, 132012, China. *email: rlx888@126.com

B-S model are insufficient. Products, including LG, HAA, acetol, and formic acid, are also produced during cellulose pyrolysis¹². It is widely recognized that cellulose is depolymerized via heat to make active cellulose, whereas the subsequent reaction step of activating cellulose remains controversial. Hence, Mamleev¹³ *et al.* proposed an improved model of the pyrolysis of cellulose that built on the previous model; the improved model clearly showed that there were two competing reactions in the pyrolysis process of cellulose. One reaction includes an intermediate that is formed via the E1 elimination reaction, and the other reaction produces LG and cellobiosan via transglycosylation. Furthermore, Bridgwater deduced that active cellulose is further broken into intermediates via dehydration and aromatization, resulting in the dehydration and condensation of coke and light gases through side chain radicals¹⁴. Some scholars have maintained that the production of light gases is indirectly related to the low temperature step or to anhydrous cellulose¹⁵. These kinetics models have largely simplified the complexity of the primary and secondary reactions of cellulose pyrolysis.

To support the simulation study, experiments have been proceeded for investigation of the cellulose pyrolysis. A thermogravimetric analyzer coupled with a Fourier-transform infrared spectrometer (TG-FTIR) has recently been developed and customized for pyrolysis research of the three components (cellulose, hemicellulose, lignin). For instance, Liu¹⁶ *et al.* studied the weight loss of cellulose and the evolution of typical functional groups. Using a summative law for the TG results, Biagini¹⁷ *et al.* obtained chemical composition of the biomass and predicted infrared spectrum of the volatiles. Py-GC/MS is another method widely applied to analyze the main components in the bio-oil that is produced in cellulose pyrolysis. Wang¹⁸ *et al.* have used Py-GC/MS to analyze the composition of the bio-oil in rapid pyrolysis of cellulose, by which a more refined cellulose pyrolysis model was established. Their work suggested that the remaining AC debris is rapidly pyrolyzed to form HAA and 1-hydroxy-2-propanone as well as secondary cracking gas and tar. In addition, related technology, such as scanning electron microscopy (SEM), X-ray diffraction (XRD) spectroscopy, Fourier transform infrared (FT-IR) spectroscopy, X-ray photoelectron (XPS) spectroscopy and isotope labeling method have also been performed to study the composition of small molecule products in cellulose pyrolysis^{19–22}. While experiments provided valuable insight, the complexity of cellulose pyrolysis make the reaction mechanism remains unclear. During the rapid pyrolysis process, hundreds of parallel or continuous pyrolysis pathways occur, thereby forming complex liquid products, including water, dehydrated sugar and carbonyl groups, compounds, phenols, furans, cyclopentanone, linear esters, linear alcohols, oligomers, etc. It is difficult to analyze the detailed mechanism through experiments.

Density functional theory (DFT) has been widely used to study the chemical reaction during the pyrolysis of cellulose, which clearly indicates each molecular reaction at the atomic and molecular level, and has been confirmed by relevant experimental data. Therefore, some scholars^{23–27} employed theoretical methods to study the mechanism of pyrolysis and forecast possible reaction pathways. There has been extensive efforts made with respect to simulation calculations. These efforts have focused on the characteristics of the specific products in cellulose pyrolysis^{28–30}. Dehydration reaction is the main reaction during the pyrolysis of cellulose, its formation mechanism has been widely investigated using density functional theory³¹. β -D-glucopyranose is the basic monomer of cellulose, and the monomer ring fractures during thermal cracking, which has also received more attention. In the pyrolysis reaction scheme proposed by Zhang³² *et al.*, quantum chemical theory calculations reveal that the free radical mechanism has the highest energy barrier and the levoglucosan chain-end mechanism is the lowest. Zhang³³ *et al.*, found that various characteristic chains and dehydration units were generated from three internal configurations: the internal unit, the reducing end (RE end), and the non-reducing end (NR end)³⁴. The generation mechanisms of small molecular weight products such as HAA, acetol, formic acid, acetic acid, furan, etc. have also been uncovered by density functional theory calculations and simulations^{35–38}. Assary and Curtiss³⁹ provided more details about retro-aldol reactions, which is a primary way to produce HAA. These results were confirmed by Zhang³⁹ *et al.*, who validated the important role of retro-aldol reactions in the HAA generation pathway. There has been extensive efforts on theoretical methods. However, there is a lack of integrated research on the mechanism of the initial stage of cellulose pyrolysis, a lack of comprehensive consideration of all possible pyrolysis reaction pathways, and research on these pathways to confirm the most favorable pathway. Hence, the mechanism of the initial stage of cellulose pyrolysis is still an unsolved mystery without consensus.

In this paper, rapidly pyrolyze of cellulose and cellulose has been performed on the Py-GC/MS to investigate the distribution of cellulose pyrolysis products, enabling further analysis of products and chemical structures. Cellobiose ($C_{12}H_{22}O_{11}$), a subunit of the biopolymer cellulose, has importance as a fundamental unit of structure in the field of plant structural sugars. This disaccharide can be obtained from the partial hydrolysis of cellulose resulting in $\beta(1-4)$ linkage between the two d-glucopyranose residues. Cellobiose, therefore, serves as a good model compound for exploring $\beta(1-4)$ glycosidic linkages^{40,41}. Furthermore, on the basis of experiments, the density functional theory (DFT) was applied to calculate the designed reaction pathways of cellobiose, and the geometric shapes and thermal properties of all relevant structures of these pathways were compared to select the optimal pathway for the cellulose pyrolysis reaction. The deduced cellulose pyrolysis reaction pathway opens up new ideas for exploring the mechanism of how cellulose is converted into pyrolysis products on a microscale.

Methods

Experimental details. *Materials.* Microcrystalline cellulose Avicel PH101 was purchased from Sigma-Aldrich. This material is mainly extracted from fiber-rich plants. It is a white powder that has an average particle diameter of 50 μm , and the molecular formula is $(C_6H_{10}O_5)_n$. Microcrystalline cellulose can be converted into a component sponge. In addition, another studied chemical cellobiose was commercially available from Sigma-Aldrich; the molecular formula is $C_{12}H_{22}O_{11}$, and it is a basic unit of cellulose that contains glucose monomers and glycosidic bonds. Before the experiment, the sample powder was dried in an oven at 100 °C for 2 h to remove absorbed water.

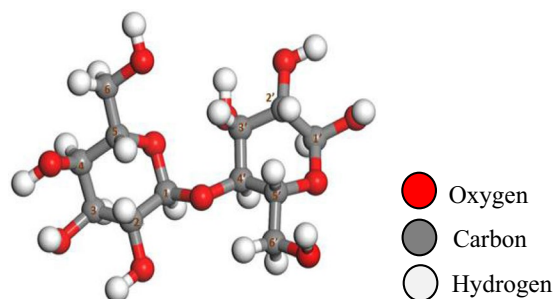


Figure 1. Optimized structure of the model compound cellobiose.

Experimental method. Cellulose and cellobiose were rapidly pyrolyzed in a Japanese Frontier EGA/PY-3030D multifunctional pyrolysis apparatus. The obtained gas phase product was analyzed using GC-MS. About 1 mg of sample was used for each experiment. The cellulose pyrolysis zone is in the range of 300–550 °C, and the maximum weight loss interval is 450–500 °C, producing plentiful volatile products⁴². It is worth noting that the high heating rate of the pyrolysis device and the poor thermal conductivity of cellulose leads to a temperature lag of about 100 °C⁴³. Therefore, the pyrolysis temperature was set as 600 °C, and this was an appropriate condition for detecting the distribution of cellulose and cellobiose pyrolysis products. In order to observe the relationship between the experimental temperatures and the product contents, the pyrolysis temperatures were set to 400 °C, 500 °C, and 600 °C, respectively.

The pyrolysis vapor released in the collector was quickly analyzed using a PerkinElmer Clarus SQ8 GC-MS. Furthermore, the temperature of the injector must be maintained at 250 °C, and the cleavage product was brought into the chromatogram using high purity helium (99.999%) as a carrier gas with a split ratio of 1:20. The column temperature of the GC/MS was programmed to increase from 50 °C (where it was held for 5 min) to 250 °C at a heating rate of 10 °C/min. Finally, the chromatographic peaks of cellulose and cellobiose were identified with reference to the NIST MS library.

Simulation details. *Simulation model.* Cellulose is a macromolecular polymer that is linked to a glucose monomer as a basic unit that incorporates a β -O-4 glycosidic bond. To reduce computation time and computational costs, the pyrolytic properties of cellulose model compounds were investigated to replace the cellulosic structures. Early works that studied cellulose pyrolysis used glucose (cellulose monomer) as a model. The pyrolysis characteristics of glucose reflect the pyrolysis process of cellulose, but it does not consider the β -O-4 glycosidic bond of the glucose monomer. Because of the highly reactive glycosidic linkages, cellobiose is more susceptible than cellulose and glucose to cleavage at higher temperatures. Combined with the experience from previous studies, cellobiose was selected as the model, and the distribution of pyrolysis products was detected using Py-GC/MS. The kinetics model of cellulose pyrolysis was established to understand the main reaction mechanism of cellulose pyrolysis. As shown in Fig. 1, cellobiose is the fundamental cyclic unit of cellulose; it contains all of the chemical components present in cellulose.

Computational method. All of the calculations in this article were done using Accelrys's Materials Studio DMol3. The dual value plus d function basis set (DND) was chosen, and the energies associated with the reactant (R), product (P), and transition state (TS) were calculated using a modified functional gradient approximation (GGA) function in the Review-Perdew-Burke-Ernzerhof (RPBE) functional. The convergence criteria for energy, force, and displacement were 2×10^{-5} Hartree (Ha), 0.004 Ha^{-1} , and 0.005 \AA , respectively. In addition, the SCF tolerance was 1×10^{-5} Ha. A number of scholars have pointed out the synergistic mechanism of cellulose in the rapid pyrolysis process, and hence, all of the reactions in this paper are based on synergistic reactions.

Pathway designed. The literature has mostly concentrated on explaining the initial mechanisms of cellulose pyrolysis, particularly the depolymerization of cellulose chains and the configuration of various small molecule products. Cellulose pyrolysis mainly produces three substances: (1) furans, (2) pyrans, and (3) linear small molecules. The foremost pyrolysis products include levoglucosan (LG), glycolaldehyde (HAA), and 5-hydroxymethyl-furan (5-HMF). The dehydration reaction that is caused by the carbonization of cellulose molecules with increased pyrolysis temperature is also an indispensable reaction. On the basis of the related theories of cellulose pyrolysis that have been previously published along with experimental research and simulation calculations, 11 reaction pathways that may occur during the thermal reaction of cellobiose are proposed. Figure 2 shows four kinds of reaction pathways of cellobiose pyrolysis, including the reactions that generate LG, HAA, 5-HMF, and dehydration reaction. Pathways 1–4 are the formation pathways of levoglucosan in cellulose pyrolysis. Among several predominant cellulose pyrolysis products⁴⁴, LG is an authority pyrolysis primary product^{45,46}; it is also an intermediate for the formation of other products^{47,48}. Pathways 5–8 are process in which a hydroxyl group on a different carbon atom reacts with H to form a water molecule and then undergoes dehydration to generate a new product. Biomass pyrolysis experiments^{49,50} indicate that dehydration mainly occurs in the preliminary stages of biomass pyrolysis. Pathways 9 and 10 lead to reactants via dehydration, cleavage, and isomeric formation of glycolaldehyde HAA. Piskorz⁵¹ *et al.* believed that the two carbon fragments that are generated via the cleavage of cellulose monomers during pyrolysis are converted to HAA. As one of the main products of

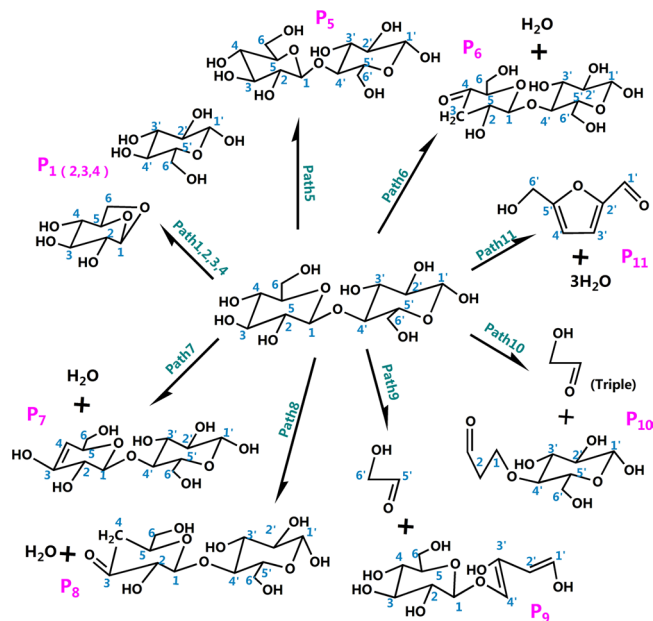


Figure 2. Reaction pathway of cellobiose pyrolysis.

cellulose pyrolysis, 5-HMF is produced via three dehydration steps of hexose on the whole. The reactants in pathway 11 undergo repeated dehydration via the fructofuranose-intermediate-mechanism to form 5-HMF, which undergoes three basic reactions of ring opening, ring formation, and dehydration.

Results and Discussion

Pyrolysis product analysis. Birot⁵² showed that cellulose and cellobiose appear to have similar thermogravimetric weight loss curves. The maximum weight loss rate reached 80% when the pyrolysis temperature was 400 °C. Table 1 lists the main products of the rapid pyrolysis of cellulose and cellobiose. Table 1 shows that when cellulose and cellobiose were pyrolyzed at 400 °C, 500 °C, and 600 °C respectively, the distribution of various products during the pyrolysis is consistent, but the content of the products is disparate. At different temperatures, the content of various products and the temperature did not show obvious rules. On the basis of experimental results, all of the products can be classified into three types: pyrans (LG), furans (5-HMF, furfural), and linear small molecule compounds (CO₂, acetaldehyde, acetic acid, etc.). Because the furan ring is more stable than the pyran ring, there tends to be more furan than pyran produced during pyrolysis⁵³. During pyrolysis of cellulose, the pyran ring may be thermally broken to generate an intermediate, and the intermediate is further cyclized to form a furan ring; the small molecule product is then further cleaved to form HAA, propionic acid, acetaldehyde, and the like. LG has the highest content of the product in the pyrolysis process, and the content of LG is quite diverse in cellulose and cellobiose; this is consistent with the theory that the production of LG is related to the degree of polymerization of the cellulose chains. The high degree of polymerization results in higher content of LG in cellulose than in cellobiose. Remarkably, in cellobiose, the content of furan substances (such as 5-HMF and furfural) is higher than in cellulose. The yield of small molecule products in pyrolysis of cellobiose is higher than that produced by pyrolysis of cellulose. The experimental results reveal that LG and 5-HMF in cellulose pyrolysis products are significant products. Hence, the simulation part of this paper focuses on the production process and reaction energy barrier.

Optimized geometries of reactant, transition state, and product. Before the molecular dynamics simulation, the reactants, intermediates, and products were geometrically optimized to search for the lowest energy points. To ensure the accuracy of the established cellulose pyrolysis model, the transition state of geometry optimization was determined using a TS search, and the identical basis set was used to calculate the reactant (R), intermediate (IM), product (P), and transition state (TS). Vibrational frequency analysis shows that the transition state has only one virtual frequency, whereas the reactants, intermediates, and products have no virtual frequencies. Structural parameter information of the optimized reactant, product, and transition state structure in each pathway are listed in Tables 2–7.

Thermodynamic analysis of pyrolysis reaction process. For the purpose of developing an in depth understanding of the energy transformation during the pyrolysis of cellulose, the thermodynamic parameters ΔH^\ominus and ΔG^\ominus of the optimized reactants and products of thermal cracking reactions at disparate pyrolysis temperatures (298, 500, 650, 800, and 950 K) were then calculated. The standard thermodynamic change in ΔH is the thermodynamic amount of the product minus the reactant, and the residual is zero-point corrected. The relevant thermodynamic parameters of the reactants and products in the 12 pathways at different reaction temperatures are summarized in Table 8. Analysis of the relationship between ΔH^\ominus and temperature is shown in Table 8. It is

Residue Time (min)	Compound	Formula	400 °C		500 °C		600 °C	
			Cellulose	Cellulose	Cellulose	Cellulose	Cellulose	Cellulose
3.03	Carbon dioxide	CO ₂	1.204	3.138	2.436	2.370	1.67	4.08
3.15	Acetaldehyde	C ₂ H ₄ O	0.618	0.182	0.283	0.432	0.39	0.81
3.41	1-Propen-2-ol, acetate	C ₅ H ₈ O ₂	0.589	0.438	1.256	1.451	1.72	2.12
3.81	Methacrolein	C ₄ H ₆ O	0.003	0.295	0.088	0.142	0.33	0.2
3.95	Acetic acid ethenyl ester	C ₄ H ₆ O ₂	0.006	0.434	0.139	0.302	0.63	0.68
4.09	Furan, 3-methyl-	C ₅ H ₆ O	0.050	0.407	0.237	0.414	0.22	0.37
4.22	Acetic acid	C ₂ H ₄ O ₂	0.032	0.519	0.201	0.614	0.17	0.66
4.95	2-Propanone, 1-hydroxy-	C ₃ H ₆ O ₂	0.0409	0.295	0.393	0.056	0.5	1.18
5.43	2,3-Pentanedione	C ₅ H ₈ O ₂	0.002	0.0690	0.0218	0.019	0.05	0.1
6.03	2-Vinylfuran	C ₆ H ₆ O	0.034	0.095	0.103	0.099	0.03	0.17
7.23	2(5H)-Furanone	C ₄ H ₄ O ₂	0.034	1.404	0.056	2.030	0.05	0.26
7.66	Propanoic acid, 2-oxo-, methyl ester	C ₄ H ₆ O ₃	0.037	0.265	0.175	0.443	0.17	0.62
8.38	3-Furaldehyde	C ₅ H ₄ O ₂	0.026	0.023	0.044	0.068	0.06	0.06
8.91	Furfural	C ₅ H ₄ O ₂	0.777	4.207	1.098	5.4245	0.95	4.16
9.06	2-Amino-1,3,5-triazine	C ₃ H ₄ N ₄	0.015	0.150	0.078	0.216	0.03	0.33
9.73	2-Propanone, 1-(acetyloxy)-	C ₅ H ₈ O ₃	0.139	0.368	0.189	0.266	0.13	0.43
11.49	1,2-Cyclopentanedione	C ₅ H ₆ O ₂	0.304	0.655	0.532	0.104	0.63	1.21
11.73	2,5-Furandione, dihydro-3-methylene-	C ₅ H ₄ O ₃	0.0129	0.031	0.050	0.064	0.02	0.03
12.22	5-Methyl-furfural	C ₆ H ₆ O ₂	0.035	0.697	0.239	1.042	0.28	1.16
13.26	Oxazolidine, 2,2-diethyl-3-methyl-	C ₆ H ₁₇ NO	0.621	0.389	0.891	0.649	0.53	0.26
13.79	1,2-Cyclopentanedione, 3-methyl-	C ₆ H ₈ O ₂	0.091	0.230	0.226	0.484	0.46	0.47
15.00	2,5-Dimethyl-4-hydroxy-3(2H)-furanone	C ₆ H ₈ O ₃	0.013	0.213	0.732	1.083	0.52	0.58
15.61	Maltol	C ₆ H ₆ O ₃	0.014	0.139	0.127	0.198	0.13	0.14
16.47	4H-Pyran-4-one, 2,3-dihydro-3,5-dihydroxy-6-	C ₆ H ₆ O ₄	0.213	1.121	0.327	1.176	0.15	0.45
17.20	4H-Pyran-4-one, 3,5-dihydroxy-2-methyl-	C ₆ H ₆ O ₄	0.360	0.897	1.308	1.337	1.5	0.85
17.53	5-Hydroxymethylfurfural	C ₆ H ₆ O ₃	0.705	18.444	1.329	21.537	1.55	11.6
21.97	D-Allose	C ₆ H ₁₂ O ₆	0.588	2.488	2.083	4.931	8.2	1.25
23.84	Levogluconan (LG)	C ₆ H ₁₀ O ₅	66.185	52.849	79.607	44.021	75.89	35.71
24.83	1,6-Anhydro-α-D-galactofuranose	C ₆ H ₁₀ O ₅	27.250	9.557	5.749	9.029	3.03	4.96

Table 1. Main products of rapid pyrolysis of cellulose and cellobiose (% in relative area).

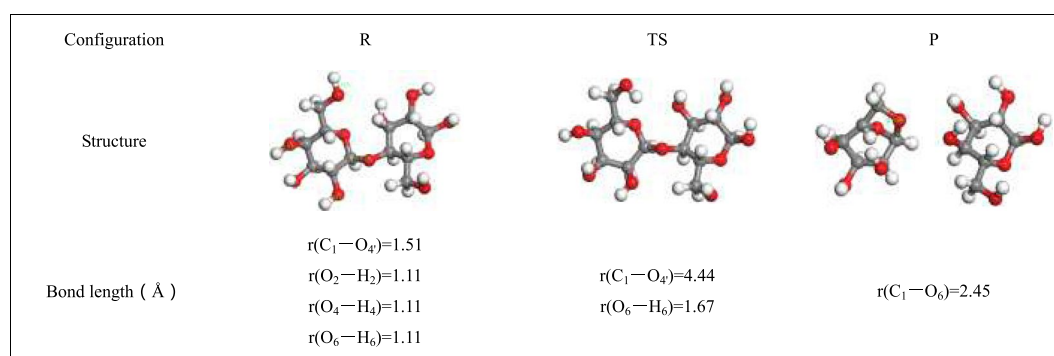


Table 2. Optimized configuration in pathway 1.

known that the correlation between ΔH^θ and temperature is not closely related. Also, the ΔH^θ values of partial pathways increase with respect to temperature; nevertheless, the section barely changes during heating.

The Gibbs free energy (ΔG^θ) is also an essential thermodynamic parameter. ΔG^θ is the thermodynamic correlation between reaction spontaneity and reactant conversion. When $\Delta G^\theta < 0$, a reaction can be carried out spontaneously. Figures 3 and 4 are graphs that show the relationship between ΔG^θ and the temperature of the 12 reaction pathways. From comprehensive analysis of Table 8 and Figs. 3 and 4, it can be inferred that as the pyrolysis temperature gradually increases, the ΔG^θ values of all of the reactions decrease, and this also explains the phenomenon that high temperature favors cellulose pyrolysis. When the temperature is lower than 500 K, the ΔG^θ values for pathways 1–4 are a relatively stable value. At this stage, the thermal effect is not significant because of the lower temperature, and this is consistent with the first stage of the thermogravimetric analysis of cellulose. When the temperature is higher than 500 K, ΔG^θ begins to decrease, and this indicates that when the temperature surpasses 500 K,

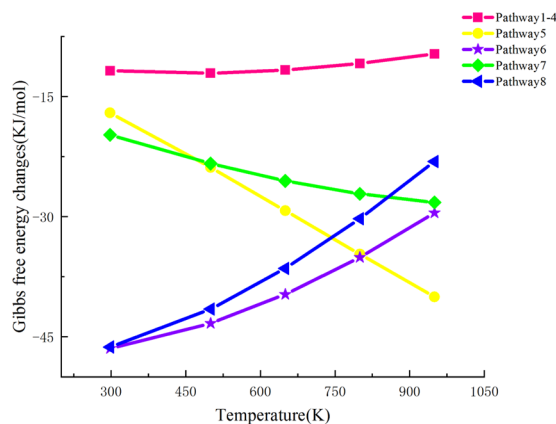


Figure 3. Gibbs free energy ΔG relationship diagram for pathway 1–8.

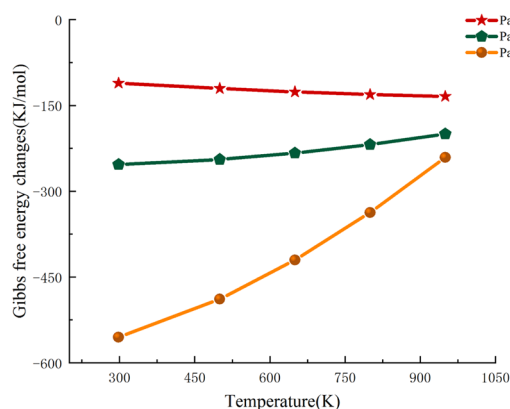


Figure 4. Gibbs free energy ΔG relationship diagram for pathway 9–11.

Configuration	TS _{2,1}	IM _{2,1}	TS _{2,2}	IM _{2,2}	TS _{2,3}	IM _{2,3}
Structure						
Bond length (Å)	$r(O_4-H_4)=0.98$ $r(C_1-O_4)=1.41$	$r(O_2-H_2)=1.11$	$r(O_4-H_2)=1.00$ $r(O_2-H_2)=1.88$	$r(O_4-H_2)=1.11$	$r(C_1-H)=3.91$	$r(C_1-H)=1.14$ $r(O_6-H_6)=1.11$
Configuration	TS _{2,4}	IM _{2,4}	TS _{2,5}			
Structure						
Bond length (Å)	$r(O_6-H_6)=5.34$ $r(O_2-H_6)=0.98$	$r(C_1-H)=1.14$ $r(O_2-H_6)=1.11$	$r(C_1-H)=1.11$			

Table 3. Optimized configuration in pathway 2.

the thermal decomposition of cellobiose produces LG. This is consistent with the theory obtained by the previous researchers who found that the main cellulose pyrolysis range is 550K–800K. It is said that the reactions between LG and HAA are competitive, and therefore, the thermodynamic quantitative values of pathways 1–4, which produce LG, are compared to pathways 10–11, which produce HAA. Because $\Delta H_{1-4}^{\ominus} < \Delta H_{10-11}^{\ominus}$, pathways 10–11, which generate LG, are more likely to occur than pathways 1–4, which generate HAA. However, $\Delta G_{1-4}^{\ominus} < \Delta G_{10-11}^{\ominus}$ indicates that the production of LG via pyrolysis is superior to the yield of HAA, and this corresponds to the theory that LG is the most significant product in the pyrolysis process of cellulose.

Pathway 1 : LG-1

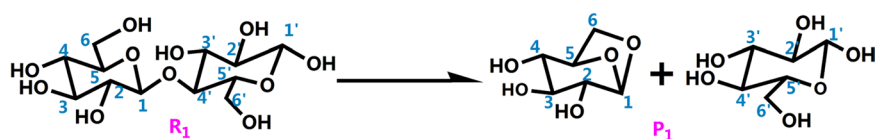


Figure 5. Pathway 1 reaction process.

Pathway 2 : LG-2

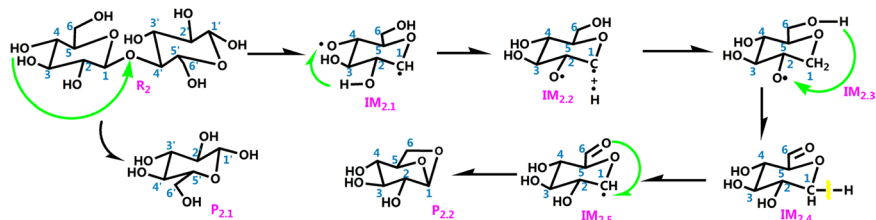


Figure 6. Pathway 2 reaction process.

Pathway 3 : LG-3

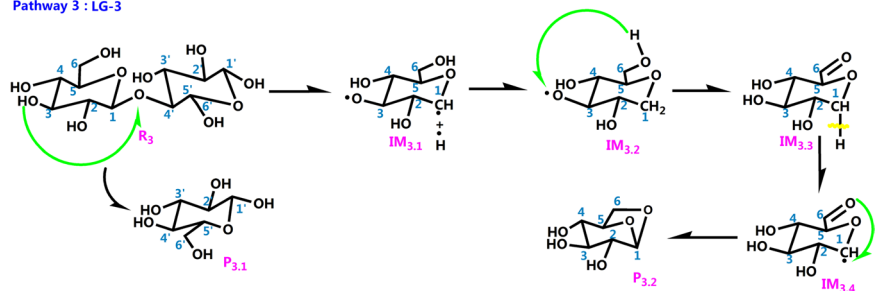


Figure 7. Pathway 3 reaction process.

Kinetic analysis of the pyrolysis process of each pathway. *Generating pathways of main product LG.* The activation energy values of the 12 reaction pathways in this work were determined based on the transition state theory. In light of transition state theory, the smallest energy discrepancy between the saddle point on the potential energy surface (i.e., the transition state) and the reactant represent the activation energy. In the following pathways, R represents a reactant, TS represents a transition state, IM represents an intermediate, and P represents a product. Moreover, in the intermediate Im a.b, a represents the number of pathways and b represents the order of object in the pathways. For instance, IM_{2,1} represents the first intermediate of the second pathway, and IM_{3,2} represents the second intermediate of the third pathway, and so on.

The first pathway is the pathway of LG generated by the synergistic reaction of cellobiose summarized by the predecessors. Some scholars believed that this pathway is the optimal pathway. In consequence, this paper chose this pathway as a comparison with other pathways that generated LG. Besides, in order to reduce the errors caused by the calculation basis set and parameter settings between the pathways that generated LG, all reaction pathways in this article were calculated using a unified basis set and calculation parameters. Under this premise, the obtained energy barrier of pathway 1 is more favorable for comparison with the energy barriers of other paths that generated LG in the paper. As shown in the Fig. 5, the H atom of the C₆-OH hydroxyl group transfers to the glycosidic bond in cellobiose, and the glycosidic bond cooperatively cleaves. The bond length of r(C₁-O₆) is 1.51 Å in R₁, and this becomes 4.44 Å in TS₁. At the same time, C₆-O₆ connects to C₁ to construct LG with a bond length r(C₁-O₆) of 2.45 Å. The activation energy of Pathway 1 is 327 kJ/mol, and this is slightly different from the value (377.54 kJ/mol) calculated by Huang *et al.* The differences in the model compound construction, dihedral angles, molecular bond lengths, and different basis functions lead to this difference.

Figure 6 shows the process by which cellobiose produces LG via pathway 2. The first step in the reaction is the simultaneous cleavage of the glycosidic bond and the H atom of -O₆H to form intermediate IM_{2,1} which contains C₄-O₆. The IM_{2,2} is generated via the transfer of H atom from O₂-H₂ to C₄-O₆. The energy barrier of this reaction step is 140.64 kJ/mol, which illustrates that the reaction process of pathway 2 is an endothermic reaction. The length of O₆-H₆ increases from 1.11 Å in IM_{2,3} to 5.34 Å in IM_{2,4}. The new bond C₆=O is about to form when H₆ shifts to C₂-O₆ in IM_{2,4}. The activation energy of the reaction step is as high as 449.66 kJ/mol, and this requires absorbing even more heat. Then, the H group that is initially bound to C₁ is removed to compose IM_{2,5}. At the end of the reaction, C₆=O bonds to C₁ to form the pyrolysis product P_{2,2} (LG). Pathway 2 follows the free-radical

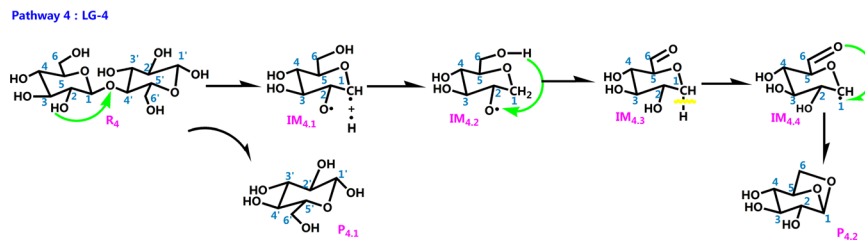


Figure 8. Pathway 4 reaction process.

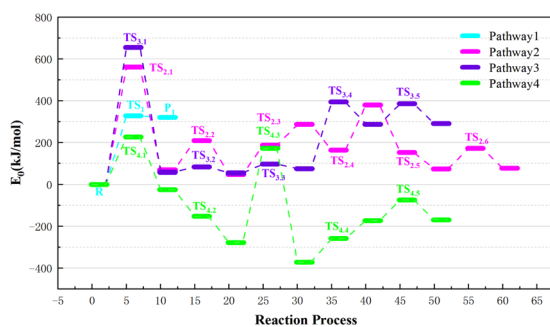


Figure 9. Reaction energy barrier diagram of pathway 1-4.

Configuration	TS _{3,1}	IM _{3,1}	TS _{3,2}	IM _{3,2}
Structure				
Bond length (Å)	$r(O_4-H_4)=0.98$ $r(C_1-O_4)=3.58$	$r(O_6-H_6)=1.11$	$r(C_1-H)=1.11$	$r(C_1-H)=1.14$ $r(O_6-H_6)=1.11$
Configuration	TS _{3,3}	IM _{3,3}	TS _{3,4}	
Structure				
Bond length (Å)	$r(O_6-H_6)=0.98$ $r(O_4-H_6)=2.84$	$r(O_4-H_6)=1.11$ $r(C_1-H)=1.14$	$r(C_1-H)=3.46$	

Table 4. Optimized configuration in pathway 3.

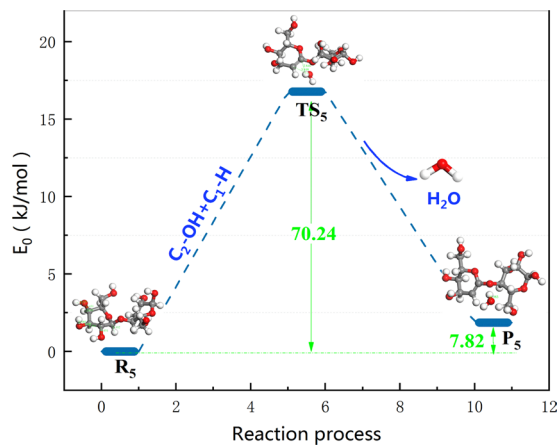


Figure 10. Reaction step and reaction energy barrier of pathway 5.

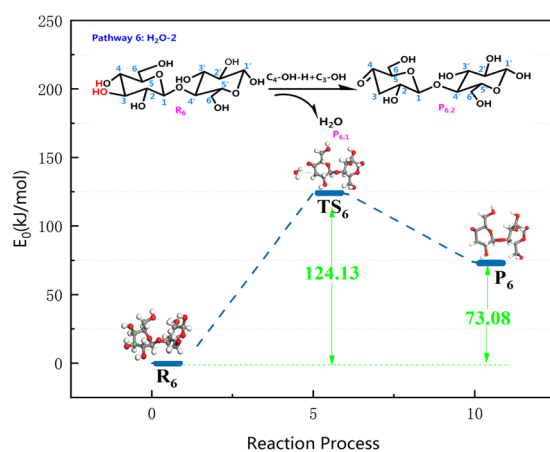


Figure 11. Reaction step and reaction energy barrier of pathway 6.

Configuration	TS _{4,1}	IM _{4,1}	TS _{4,2}	IM _{4,2}
Structure				
Bond length (Å)	$r(\text{O}_2-\text{H}_2)=3.64$ $r(\text{C}_1-\text{O}_4)=3.81$ $r(\text{C}_1-\text{O}_2)=2.43$	$r(\text{C}_1-\text{O}_2)=1.86$	$r(\text{C}_1-\text{H})=1.10$	$r(\text{O}_6-\text{H}_6)=1.11$ $r(\text{C}_1-\text{H})=1.14$
Configuration	TS _{4,3}	IM _{4,3}	TS _{4,4}	
Structure				
Bond length (Å)	$r(\text{O}_6-\text{H}_6)=5.34$	$r(\text{O}_2-\text{H}_6)=1.11$ $r(\text{C}_1-\text{H})=1.14$	$r(\text{C}_1-\text{H})=1.09$	

Table 5. Optimized configuration in pathway 4.

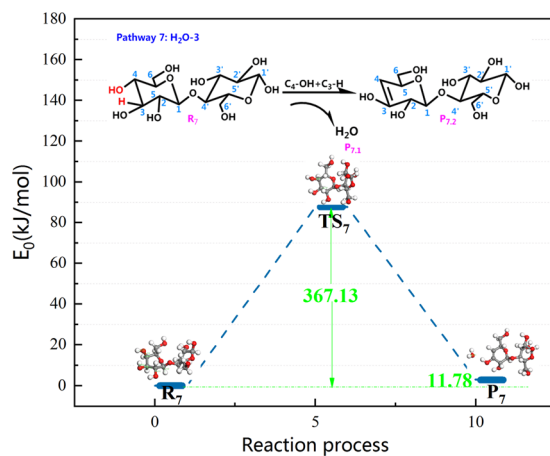


Figure 12. Reaction step and reaction energy barrier of pathway 7.

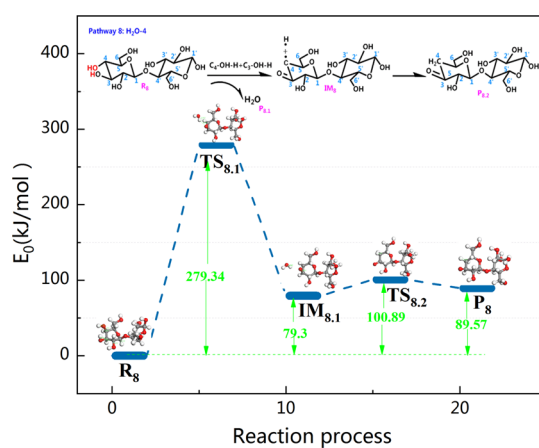


Figure 13. Reaction step and reaction energy barrier of pathway 8.

mechanism of LG, and the cellulose chain is first broken into an anhydroglucose group in the pyrolysis of cellulose; this is then converted to levoglucosan. Free radicals formed via homogeneous cleavage of cellulose chains.

Pathway 2 is similar to the first step of pathway 3, and the same is true for C_1 and cleavage of the glycosidic bond. Figure 7 gives the reaction process of pathway 3 in cellulose pyrolysis. In the energy barrier diagram, the highest energy barrier in each pathway is shown. This indicates that this step is the rate-determining step for the whole levoglucosan formation process, which occurs via a free-radical mechanism. In the course of pyrolysis, a mass of free H groups concatenate to unsaturated C_1 to form C_1-H for $IM_{3,2}$. Thereafter, H transfers from C_6-OH to C_4-O , the bond O_4-H_6 lengthens to form $TS_{3,3}$, and the length of O_4-H_6 shortens from 2.84 Å to 1.11 Å. These observations indicate that the transition state $TS_{3,3}$ generates a new bond O_4-H_6 that is present in $IM_{3,3}$. It can be referred to Fig. 7 that the $IM_{3,3}$ reacts to $P_{3,2}$ through breaking C_1-H bond plus O_6 shifts from C_6 to C_1 and forming O_6-C_1 .

Form Fig. 8, O_2-H_2 breaks as the pyrolysis temperature increases, glucopyranose forms in pathway 4. At the same time, consistent with the sharp decrease of $r(C_1-O_2)$ from 2.43 Å to 1.86 Å, it can be inferred that the unsaturated O_2 that lost an H atom then connects with C_1 . Heat in the amount of 226.15 kJ/mol is absorbed to form intermediate $IM_{4,1}$. In the pyrolysis reaction, the H group combines with C_1 to produce intermediate $IM_{4,2}$, wherein the new bond $r(C_1-H)$ is 1.14 Å. The C_6-OH breaks directly by adjacent H atoms transfer shown in Fig. 8. Specifically, the H_6 atom moves from C_6-OH to C_2-O to form a hydroxy group (O_2-H_2) and $C_6=O$ bond in $IM_{4,3}$, respectively, through $TS_{4,3}$; and O_6 atom transfers from C_6 to C_1 to generate C_1-O_6 in $P_{4,2}$, via $TS_{4,5}$. The energy of the glycosidic bond cleavage in the first step of pathway 4 consumed less energy than pathways 2 and 3, and this is consistent with the energy of 155–228 kJ/mol that is obtained in the experiment⁵⁴. This verifies the rationality of this step.

Analyzing the change in activation energy during each reaction enables us to develop further kinetic analysis. Figure 9 shows potential energy curves for pathways 1–4; the curves depict the changes in thermodynamic energy in each pyrolysis pathway that leads to LG. The energy barriers in the graph indicate the reaction energy of the transition state relative to that of the reactants, and the reaction energy is equal to difference between the product and reactant energy. In this article, there are four calculations about the pathway of LG generation. The first one is the pathway for synergistic reaction of cellobiose summarized by previous generations to generate LG. It is more

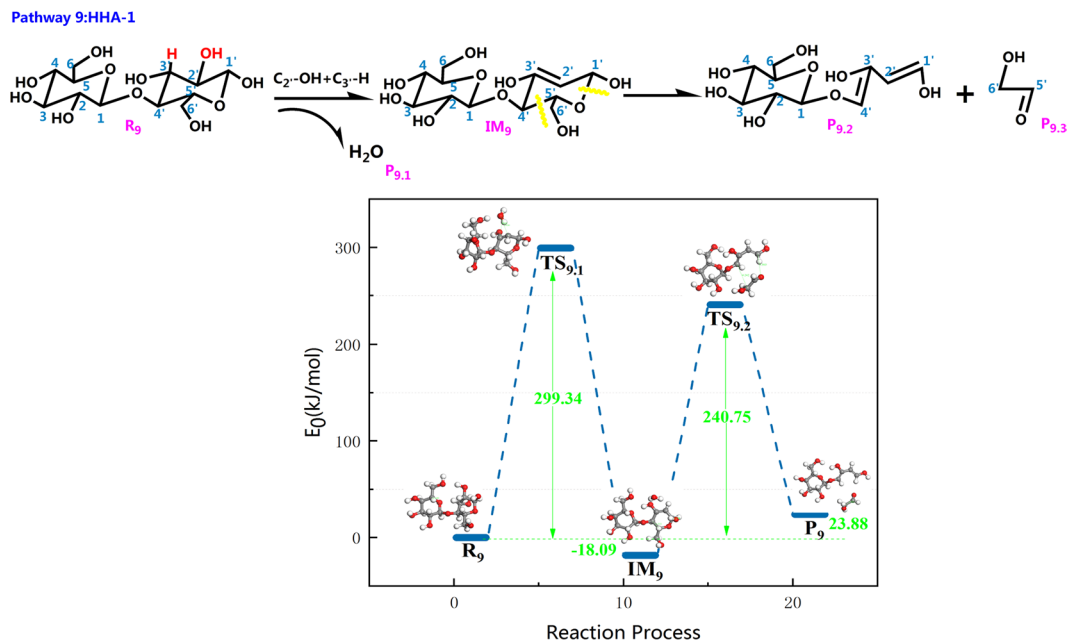


Figure 14. Reaction step and reaction energy barrier of pathway 9.

Configuration	R	TS ₅	P ₅	TS ₆	IM ₆
Structure					
Bond length (Å)	$r(\text{C}_2-\text{OH})=1.43$ $r(\text{C}_3-\text{H})=1.10$ $r(\text{C}_3-\text{OH})=1.44$ $r(\text{C}_4-\text{H})=1.11$ $r(\text{C}_4-\text{OH})=1.45$ $r(\text{O}_3-\text{H})=0.99$ $r(\text{C}_1-\text{H})=1.10$ $r(\text{O}_4-\text{H})=0.98$	$r(\text{C}_2-\text{OH})=3.85$ $r(\text{C}_1-\text{H})=2.85$	$r(\text{O}_2\text{H}-\text{H})=0.98$	$r(\text{C}_3-\text{OH})=3.64$ $r(\text{O}_4-\text{H})=1.77$	$r(\text{O}_3\text{H}-\text{H})=1.00$
Configuration	P ₆	TS ₇	P ₇	TS _{8,1}	IM ₈
Structure					
Bond length (Å)	$r(\text{C}_3-\text{H})=1.10$	$r(\text{C}_4-\text{OH})=1.46$ $r(\text{C}_3-\text{H})=1.13$	$r(\text{O}_4\text{H}-\text{H})=0.98$	$r(\text{C}_4-\text{OH})=3.06$ $r(\text{O}_3-\text{H})=2.19$	$r(\text{C}_3=\text{O})=1.46$ $r(\text{O}_4\text{H}-\text{H})=0.98$
Configuration	TS _{8,2}	P ₈			
Structure					
Bond length (Å)	$r(\text{C}_4-\text{H})=1.10$	$r(\text{C}_4-\text{H})=1.14$			

Table 6. Optimized configuration in pathway 5–8.

convenient to compare with other energy barriers in the paper to generate LG. In this paper, the authors designed routes 2, 3, and 4 in strict accordance with the principle that H on different hydroxyl –OH groups was transferred to glycosidic bonds, which caused the glycosidic bonds to break. Combining with previous studies, the former usually only considered the cooperative cleavage of H and glycosidic bonds on the C₆–OH hydroxyl group, while

Pathway 10:HHA-2

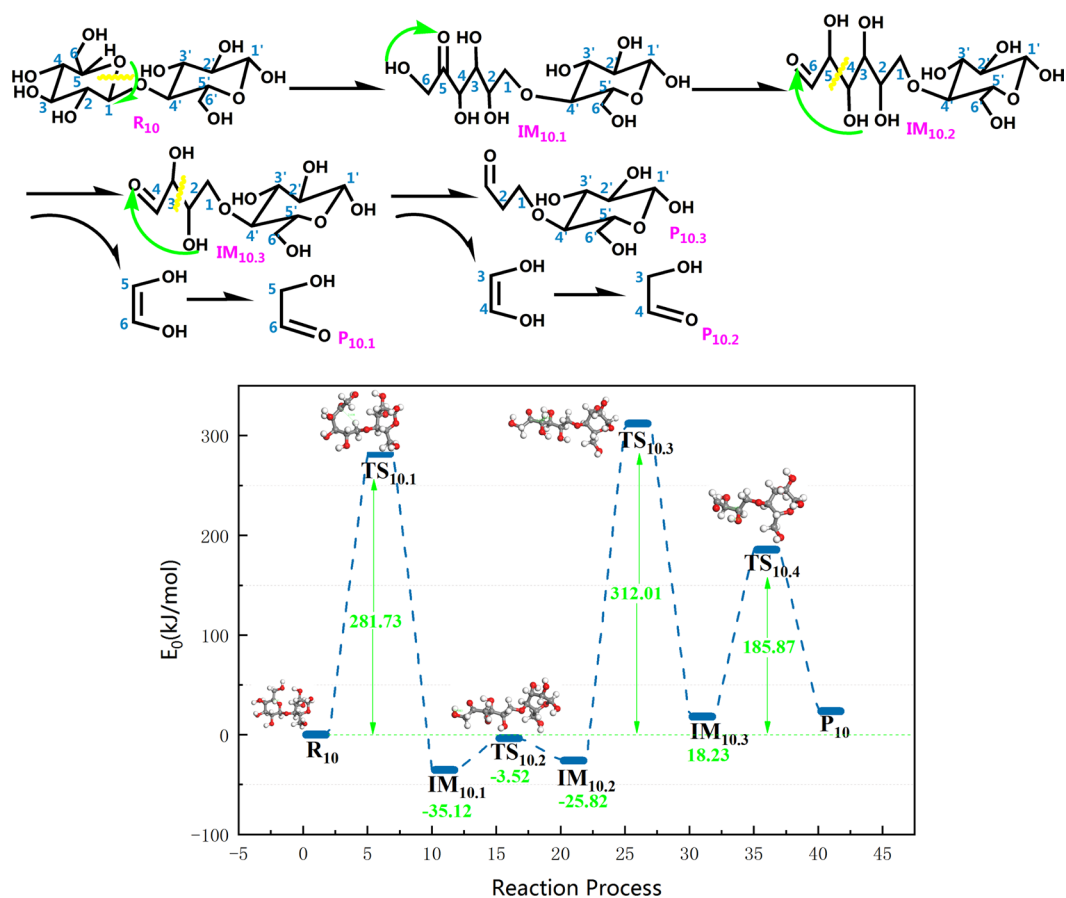


Figure 15. Reaction step and reaction energy barrier of pathway 10.

pathways 2, 3, and 4 in this article considered the reaction of H with glycosidic bond cleavage. In pathway 2, the H on the hydroxyl group of C₄ was broken, and the H radical moved to the glycosidic bond to bind. Since the H radical moved far away, the heat absorbed during the reaction was as high as 560.81 kJ/mol, which was more difficult to achieve. Similar to Pathway 2, the free radical formed by the H cleavage on the hydroxyl group of C₃ in Pathway 3 moved to the glycosidic bond far away, which caused a large amount of energy of 655.37 kJ/mol to be absorbed in this step reaction. Although the path design of pathways 2 and 3 was strictly based on the principle of the combination of H radicals that were shed from the hydroxyl groups in cellobiose and glycosidic bonds, the energy of the H radicals in pathways 2 and 3 to break from C₃-OH and C₄-OH was not favorable. Hence, the cellobiose does not react according to pathways 2, 3 during the actual reaction. The H radical shed from the hydroxyl group of C₂ in the pathway 4 moved to the glycosidic bond, and absorbed 226.15 kJ/mol of heat, and this step is the rate determining step of the entire reaction pathway 4. As calculated by Assary⁵⁵ *et al.*, Zhang⁵⁶ *et al.*, the comparison of the results shows that the path design of path 4 is more reasonable, and cellobiose may react to generate LG according to this path. Compared with the rate-determining step of absorption of 327.47 kJ/mol heat in pathway 1, the rate-determining step of pathway 4 is 226.15 kJ/mol. It can be inferred that in the process of cellobiose cracking to generate LG, pathway 4 is a valid competing path for pathway 1.

Dehydration reaction pathway. Carbohydrates have a large amount of hydroxyl -OH and are the dominant component of biomass, and thus, dehydration during cellulose pyrolysis is inevitable. From previous experience, it is known that the 1,2 dehydration mechanism and 1,3 dehydration mechanism are the most pervasive, more so than in alcohol dehydration^{57,58}. Some scholars⁵⁹ have proposed the hydrogen bonding-assisted Grob fragmentation mechanism and hydrogen bond-assisted pyran ring recombination mechanism to understand the dehydration phenomenon in biomass. Regarding the choice of mechanism, this study used the most widespread mechanism for analyzing the dehydration reaction and its product distribution during cellulose pyrolysis.

Pathway 5 abides by the 1,2 dehydration mechanism. The reaction step and reaction energy barrier of pathway 5 are summarized in Fig. 10. First, the H on C₁ and the -OH on C₂ are cleaved. Then, C₁-H combines with C₂-OH to generate water molecules, absorbing 70.24 kJ/mol of heat during the reaction, which existed disparity with the activation energy of 305.3 kJ/mol when glucopyranose was dehydrated that Zhang⁶⁰ *et al.* Differences in the choice of model compounds and reaction conditions are the cause of differences in activation energy.

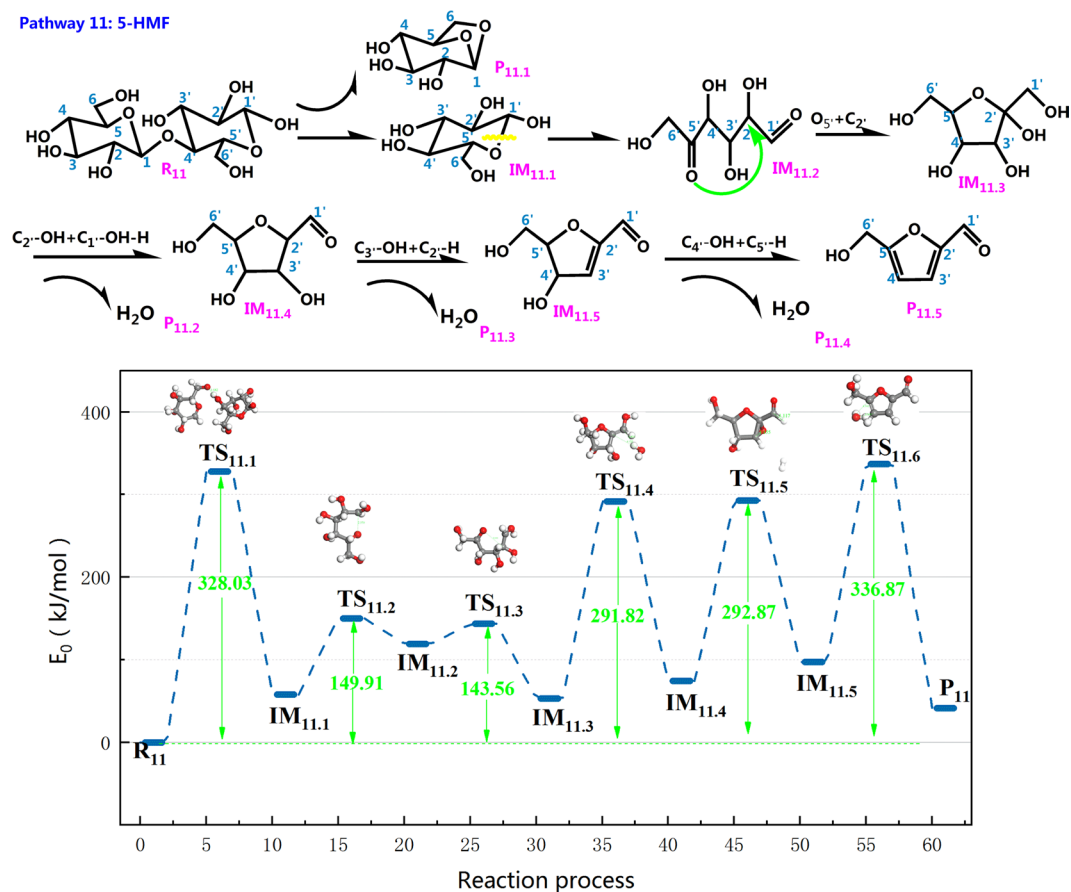


Figure 16. Reaction step and reaction energy barrier of pathway 11.

Paine III *et al.* proposed a hydrogen bond-assisted Grob fragmentation mechanism for carbohydrate pyrolysis. A similar mechanism can be derived from this. Also, hydrogen bonding assistance in the rearrangement of pinacol is another possible way for dehydration of $-O_2H$ in cellobiose. In pathway 6, the H of C_4-OH combines with the dehydration of C_3-OH shown in Fig. 11, and then the H on the hydroxyl-OH on C_4 cleaves to generate P_6 with a $C_4=O$. With the release of 124.13 kJ/mol of heat, the activation energy of this reaction is lower than the other dehydration pathway in this paper. Therefore, it can be extrapolated that this pathway is the main dehydration process apart from pathway 5. The unsaturated C_3 bond in R_6 links to the free H radicals during pyrolysis to produce saturated P_6 .

Figure 12 shows an overview of the pyrolysis process and the potential energy of cellobiose pathway 7. This pathway was a dehydration process with a lower energy barrier proposed by the predecessors. It is competitive in the pathway of cellulose dehydration reaction. Therefore, in this paper, the theoretical study of pathway 7 was carried out with the same base group and calculation parameters, which was beneficial to compare with the dehydration pathway designed by the author. It is conducive to select the optimal path for dehydration reaction. Pathway 7 displays 1,2-dehydration of C_4-OH and C_3-H , and the bond length of the participating reaction in TS_7 merely changes by 0.03 Å compared to that in reactant R_7 . It can be deduced that the response rate of pathway 7 tends to be slow, and hence, there was no significant change in the bond length in TS_7 . Throughout the reaction shown in Fig. 12, 367.13 kJ/mol of heat is released. Nimilos⁶¹ *et al.* proposed that the 1,2 dehydration barrier of simple alcohols and LG is about 67–69 kcal/mol (280.46–288.83 kJ/mol); however, 367.13 kJ/mol of heat is released during the reaction that follows pathway 7. Obviously, there is a certain difference in the energy barrier. For analysis, it is determined that the structure of cellobiose itself is more tangled than that of LG. The reaction structure is erratic when it goes through TS_7 in the reaction, and the reaction rate is sluggish, which indirectly induces an increase in the reaction barrier. Thus, this causes the discrepancy in activation energy during the process. From the energy barrier figure, it can be inferred that H leaving C_3 is the rate determining step of the pathway.

Taking into account the diversity of the reaction steps in pyrolysis of cellulose, pathway 8 is unlike the other dehydration pathways. The other dehydration reactions were synergistic reactions without intermediates, whereas pathway 8 leads to intermediate IM_8 . The reaction step and reaction energy barrier of pathway 8 are shown in Fig. 13. It then joins the H radical to form saturated P_8 . During the dehydration reaction of pathway 8, hydroxy $-OH$ and H first detach from C_4 and C_3-OH , respectively. This releases 279.34 kJ/mol of heat while generating IM_8 , which has a $C_3=O$ double bond. Corresponding kinetic data have been reported with glucose as the model compound in work reported by Mayes *et al.* (E_a , 304.8–336.2 kJ/mol vs 298.6–323.4 kJ/mol). In addition, the C_4 of


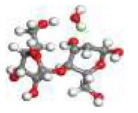

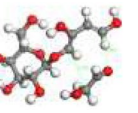
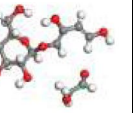

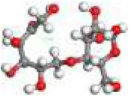
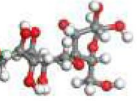
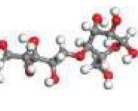

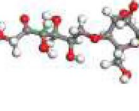
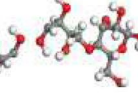
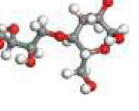
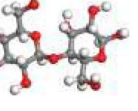
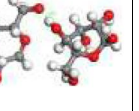



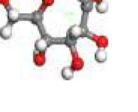
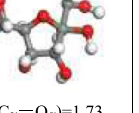
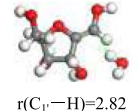


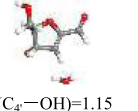
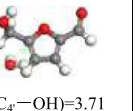
Configuration	R ₉	TS _{9,1}	IM ₉	TS _{9,2}	P ₉
Structure					
Bond length (Å)	r(C ₂ -OH)=1.44 r(C ₃ -H)=1.10	r(C ₂ -OH)=3.05 r(C ₃ -H)=4.00	r(C ₄ -C ₅)=1.55 r(C ₁ -O ₅)=1.44	r(C ₄ -C ₅)=4.24 r(C ₁ -O ₅)=3.56	r(C ₅ -C ₆)=1.52
Configuration	R ₁₀	TS _{10,1}	IM _{10,1}	TS _{10,2}	IM _{10,2}
Structure					
Bond length (Å)	r(C ₅ -H)=1.14	r(C ₅ -H)=2.61	r(O ₆ -H ₆)=1.11	r(O ₆ -H ₆)=0.98	r(O ₄ -H ₄)=0.99 r(C ₄ -C ₅)=1.53
Configuration	TS _{10,3}	IM _{10,3}	TS _{10,4}	R ₁₁	TS _{11,1}
Structure					
Bond length (Å)	r(O ₄ -H ₄)=1.11 r(C ₄ -C ₃)=1.54	r(C ₂ -C ₃)=1.54 r(O ₂ -H ₂)=1.11	r(C ₂ -C ₃)=1.57 r(O ₂ -H ₂)=1.00	r(O ₆ -H ₆)=1.11	r(O ₆ -H ₆)=1.68
Configuration	IM _{11,1}	TS _{11,2}	IM _{11,2}	TS _{11,3}	IM _{11,3}
Structure					
Bond length (Å)	r(C ₁ -O ₅)=1.51	r(C ₁ -O ₅)=2.57	r(C ₅ =O)=1.51	r(C ₂ -O ₅)=3.10	r(C ₂ -O ₅)=1.73 r(C ₁ -H)=1.14 r(C ₂ -OH)=1.72
Configuration	TS _{11,4}	IM _{11,4}	TS _{11,5}	IM _{11,5}	TS _{11,6}
Structure					
Bonlength (Å)	r(C ₁ -H)=2.82 r(C ₂ -OH)=4.12	r(C ₁ -H)=2.82 r(C ₂ -OH)=4.12	r(C ₃ -OH)=1.46 r(C ₁ -H)=1.12	r(C ₄ -OH)=1.15 r(C ₅ -H)=1.10	r(C ₄ -OH)=3.71 r(C ₅ -H)=4.35

Table 7. Optimized configuration in pathway 9–11.

IM₈ is not saturated, and therefore, the H radical that is produced in the pyrolysis process combines with C₄ and eventually produces the saturated dehydration product P₈.

Summarizing the previous experience, it can be inferred that the dehydration energy barrier during the pyrolysis of cellulose model compounds is 264.56–414.83 kJ/mol, and the dehydration energy barriers obtained by some studies were concentrated in 298.6–336.2 kJ/mol, which was closed to the energy barrier of pathway 7 (C₄-OH + C₃-H, 367.13 kJ/mol) and pathway 8 (C₄-OH-H + C₃-OH-H, 279.34 kJ/mol) calculated with density functional theory in this paper, further illustrates the rationality of the calculation results of pathways 7, 8. However, the calculated energy barriers for pathway 5 (C₂-OH + C₁-H) and pathway 6 (C₄-OH-H + C₃-OH) in this paper were 70.24 kJ/mol and 124.13 kJ/mol, as compared with Lu *et al.* and Mayes *et al.*, the calculation results of pathway 6 and 5 were more favorable in thermodynamics, which indicated that the dehydration reaction of pathway 5 and pathway 6 is more likely to occur in kinetics.

Small molecule product generation pathway. Glycolaldehyde HAA is a crucial pyrolysis product, and its yield is second only to LG in bio-oil. It is primarily derived from the cleavage of cellulose as a whole (ring breakage). Lu⁶² *et al.* considered that HAA is chiefly derived from the cleavage of C₁-C₂, C₅-C₆, C₃-C₄ in the cellulose monomer. Furthermore, a tiny fraction of HAA is generated from secondary cleavage of LG. Two reaction pathways for producing HAA are proposed in this paper, and the remarkable difference between pathways 10 and 9 is that the former incorporates a retro-diels-alder reaction.

As shown in Fig. 14, pathway 9 first goes through dehydration of cellobiose, and then C₄'-C₅' and C₁'-O₅' of cellobiose are cleaved, leading to ring opening of the pyran ring. This results in the product P₉, which has two C=C double bonds (C₁'-C₂', C₅'-C₆'), and HAA molecules (two carbon fragments) and releases 240.75 kJ/mol of heat. According to Nimols *et al.*, the energy barrier of the 1,2 dehydration process is in the range of 280–290 kJ/mol, and the calculation results in this paper are closed to this range. As seen from the combination

Pathways	Parameters(KJ/mol)	298 K	500 K	650 K	800 K	950 K
Pathway1 Pathway2	ΔH^{\ominus}	-10.42	-12.61	-14.37	-16.3	-18.38
Pathway3 Pathway4	ΔG^{\ominus}	-11.78	-12.09	-11.7	-10.87	-9.68
Pathway5	ΔH^{\ominus}	-7.92	-6.05	-5.7	-5.95	-6.59
	ΔG^{\ominus}	-17.05	-23.856	-29.27	-34.69	-40.02
Pathway6	ΔH^{\ominus}	-49.43	-53.67	-57.67	-62.29	-67.41
	ΔG^{\ominus}	-46.46	-43.34	-39.71	-35.08	-29.53
Pathway7	ΔH^{\ominus}	-14.18	-15.34	-17.34	-19.99	-23.05
	ΔG^{\ominus}	-19.79	-23.38	-25.54	-27.15	-28.23
Pathway8	ΔH^{\ominus}	-51.19	-56.45	-61.01	-65.99	-71.29
	ΔG^{\ominus}	-46.28	-41.55	-36.46	-30.267	-23.11
Pathway9	ΔH^{\ominus}	-96.3	-98.91	-103.47	-109.73	-117.25
	ΔG^{\ominus}	-110.96	-120.38	-126.25	-130.86	-134.17
Pathway10	ΔH^{\ominus}	-261.52	-274.5	-289.83	-308.65	-330
	ΔG^{\ominus}	-253.24	-244.52	-233.53	-218.57	-199.83
Pathway11	ΔH^{\ominus}	-630.87	-690.43	-749.2	-816.54	-890.2
	ΔG^{\ominus}	-555.13	-488.59	-420.24	-337.23	-240.94

Table 8. Changes in standard thermodynamic parameters at different temperature.

of the reaction steps and the potential energy profile, the pyran ring that is subjected to dehydration is more likely to undergo the ring opening reaction.

On the basis of previous results⁶², when the cellulose pyrolysis produces HAA molecules, cleavage of the C₁-O bond occurs first, causing a ring opening reaction of the cellulose monomer. In the reaction step of Fig. 15, the pyran ring opens on R₁₀, and the H atom is transferred from C₅ to C₁. Next, the H atom on O₆-H₆ is transferred to C₅=O and constructs a new O₅-H₅ bond and a C₆=O double bond. Intermediate IM_{10,2} is generated with a release of 3.52 kJ/mol of energy. Analogously, r(O₄-H₄) is 0.99 Å in intermediate IM_{10,2}, and the bond length r(O₄-H₄) increase to 1.11 Å after the transition state TS_{10,3}. Because of the longer bond length, H₄ falls off of O₄ and is then transferred to C₆=O₆. After the new double bond forms, C₄-C₅ cleavage releases heat of approximately 312.01 kJ/mol, and simultaneously produces a C₅-C₆ two-carbon small molecule fragment, which in turn undergoes a retro-diels-alder reaction to produce a small molecule of HAA. At the end of reaction process, C₂-C₃ breaks to grow new small molecule fragments and C₂=O double bonds. The small molecule fragments then continue forming HAA molecules via the retro-diels-alder reaction, and thus, the barrier is as low as 185.87 kJ/mol. Analogous pathways have been proposed by previous researchers who insisted that these pathways should mainly produce HAA. The reaction energy barrier calculated by Lu *et al.*⁶³ for the conversion of two carbon fragments to form HAA was 177.9 kJ/mol-391.3 kJ/mol. In contrast to the pathway 9 of HAA produced by the pyrolysis of cellobiose in this paper, the transition state TS_{9,1} was the process of cellobiose cleaved to generate β-d-glucopyranose, absorbing 299.34 kJ/mol of heat during the reaction. Through the transition state TS_{9,2}, the pyran ring of β-d-glucopyranose opened the ring to generate the small molecule product HAA and absorbed 240.75 kJ/mol of heat. This energy barrier was closer to the calculation of Lu *et al.*, illustrating the rationality of the HAA generation process in pathway 10. The corresponding processes of the three transition states TS_{10,1}, TS_{10,2}, and TS_{10,3} of pathway 10 in this paper are the β-d-glucopyranose formation of cellobiose glycoside bond breakage, the first HAA generated, and the second HAA generated. The corresponding energy barriers of TS_{10,2} and TS_{10,3} were 312.01 kJ/mol and 185.87 kJ/mol, which were in good agreement with the calculation results of Lu *et al.* It is concluded that cellobiose has the potential to generate HAA according to the steps designed in pathway 9,10 in this paper.

Throughout previous research, 5-HMF has been a significant product in the course of cellulose pyrolysis. Some scholars^{64,65} conducted a study on 5-HMF and its isomers and proposed that HMF is a dehydration derivative produced by dehydrating hexose three times. Figure 16 gives the reaction step and reaction energy barrier of pathway 11. There is a similarity between the first step in pathway 11 and pathway 1. The IM_{11,2} is generated via the rearrangement of IM_{11,1} with the C₁-O₅' of glucopyranose cleaves. Then, the new C₅=O double bond is about to form in a ring opening reaction. Upon going through a transition state to generate a new intermediate, O₅' and C₂' in IM_{11,2} join to form a ring. The subsequent reaction procedure is three dehydration processes, and eventually the product 5-HMF is generated. Observing the energy profile of pathway 11, the energy barriers for the three dehydrations of 5-HMF were 238.65 kJ/mol, 218.4 kJ/mol, 239.6 kJ/mol, and the energy barriers for the three dehydrations calculated by Vinus⁶⁶ were 215.58 kJ/mol, 215.58 kJ/mol, 267.90 kJ/mol, respectively. The last dehydration and cyclization occurred simultaneously, so the reaction energy barrier was higher than the other two dehydration reactions. The calculation results in this paper were close to those calculated by Vinus. It showed that pathway 11 was a possible path for cellobiose cleavage to form 5-HMF.

Conclusion

To investigate the initial mechanism of cellulose pyrolysis, we used Py-GC/MS experiments combined with DFT theory. We explored the formation mechanism of the initial stage of cellobiose pyrolysis.

Among the three types of products produced in the thermal cracking experiment, $\text{Furan}_{\text{Cellulose}} < \text{Furan}_{\text{Cellulbiose}}$, $\text{Pyran}_{\text{Cellulose}} > \text{Pyran}_{\text{Cellulbiose}}$, and the content of small molecule products in cellobiose is higher than that in cellulose. The calculation results obtained using DFT theory are in great agreement with the experimental results. From the intrinsic theoretical research and experimental results, a modified cellulose pyrolysis model is proposed, including the formation of new reactions of LG, HAA, 5-HMF, and dehydration. From a comparison of energy barriers, it is found that of the four reaction paths for producing LG, pathway 1 is the only reaction that directly generates LG through a synergistic mechanism. Also, the energy barrier of the reaction is low, and hence, pathway 1 is the optimal pathway for generating LG. In the subsequent dehydration reaction, the reaction energy barriers are arranged in increasing order as: pathways 5, 6, 7 and 8. This order indicates that the combined dehydration of $\text{C}_1\text{-H}$ and $\text{C}_2\text{-OH}$ in pathway 5 is the prime dehydration reaction during cellulose pyrolysis. Both pathways 9 and 10 are reactions in which cellulose pyrolysis produces HAA, and the HAA formation step in pathway 9 is simpler than that of pathway 10; in contrast, pathway 10 leads to higher HAA content. Finally, the reaction process of hexose to form the small molecule product 5-HMF via three dehydration steps was studied. In conclusion, the main reaction processes in the cellulose pyrolysis are pathway 1, 5, 9, and 11. This work enables further analysis of biomass energy conversion and utilization research. In addition, the pyran ring is the basic monomer structure in the long chain of cellulose. In this article, the mechanism of the pyrolysis of the pyran ring during the pyrolysis of cellulose is not sufficiently studied. In the future research, the combination of experiment and simulation will be considered to study the pyrolysis mechanism of pyran ring during cellulose pyrolysis^{67,68}.

Received: 9 December 2019; Accepted: 30 January 2020;

Published online: 27 February 2020

References

- Zhang, X. S., Yang, G. X., Jiang, H., Liu, W. J. & Ding, H. S. Mass production of chemicals from biomass-derived oil by directly atmospheric distillation coupled with co-pyrolysis. *SCI.REP-UK*. **3**, 1120, <https://doi.org/10.1038/srep01120> (2013).
- Kumagai, S. *et al.* Beech Wood Pyrolysis in Polyethylene Melt as a Means of Enhancing Levoglucosan and Methoxyphenol Production. *Sci. Rep.* **9**, 1955, <https://doi.org/10.1038/s41598-018-37146-w> (2019).
- Martin, A. F. *et al.* Altered lignocellulose chemical structure and molecular assembly in CINNAMYL ALCOHOL DEHYDROGENASE-deficient rice. *Sci. Rep.* **9**, 17153, <https://doi.org/10.1038/s41598-019-53156-8> (2019).
- Ahn, K., Schedl, A., Zweckmair, T., Rosenau, T. & Potthast, A. Fire-induced structural changes and long-term stability of burned historical rag papers. *Sci. Rep.* **8**, 12036, <https://doi.org/10.1038/s41598-018-30424-7> (2018).
- Estelle, B. *et al.* Mobility of pectin methylesterase in pectin/cellulose gels is enhanced by the presence of cellulose and by its catalytic capacity. *Sci. Rep.* **9**, <https://doi.org/10.1038/s41598-019-49108-x> (2019).
- Shen, D. K. & Gu, S. The mechanism for thermal decomposition of cellulose and its main products. *Bioresource. Technol.* **100**, 6496–6504, <https://doi.org/10.1016/j.biortech.2009.06.095> (2009).
- Elsakhawy, M. & Hassan, M. L. Physical and mechanical properties of microcrystalline cellulose prepared from agricultural residues. *Carbohydr. Polym.* **67**, 1–10, <https://doi.org/10.1016/j.carbpol.2006.04.009> (2007).
- Foyle, T., Jennings, L. & Mulcahy, P. Compositional analysis of lignocellulosic materials: Evaluation of methods used for sugar analysis of waste paper and straw. *Bioresource. Technol.* **98**, 3026–3036, <https://doi.org/10.1016/j.biortech.2006.10.013> (2007).
- Bradbury, A. G. W., Sakai, Y. & Shafizadeh, F. A kinetic model for pyrolysis of cellulose. *J. Appl. Polym. Sci.* **23**, 3271–3280, <https://doi.org/10.1002/app.1979.070231112> (2010).
- Lewin, M., Basch, A. Structure, Pyrolysis, and Flammability of Cellulose. https://doi.org/10.1007/978-1-4684-6973-8_1 (1978).
- Shafizadeh, F. & Bradbury, A. G. W. Thermal degradation of cellulose in air and nitrogen at low temperatures. *J. Appl. Polym. Sci.* **23**, 1431–1442, <https://doi.org/10.1002/app.1979.070230513> (1979).
- Radlein, D., Piskorz, J. & Scott, D. S. Fast pyrolysis of natural polysaccharides as a potential industrial process. *J. Anal. Appl. Pyrol.* **19**, 41–63, [https://doi.org/10.1016/0165-2370\(91\)80034-6](https://doi.org/10.1016/0165-2370(91)80034-6) (1991).
- Mamleev, V., Bourbigot, S. & Yvon, J. Kinetic analysis of the thermal decomposition of cellulose: the main step of mass loss. *J. Anal. Appl. Pyrol.* **80**, 151–165, <https://doi.org/10.1016/j.jaap.2007.01.013> (2007).
- Bridgwater, A. V. Principles and practice of biomass fast pyrolysis processes for liquids. *J. Anal. Appl. Pyrol.* **51**, 3–22, [https://doi.org/10.1016/S0140-6701\(00\)94648-4](https://doi.org/10.1016/S0140-6701(00)94648-4) (1999).
- Foyle, T., Jennings, L. & Mulcahy, P. Compositional analysis of lignocellulosic materials: Evaluation of methods used for sugar analysis of waste paper and straw. *Bioresource. Technol.* **98**, 3026–3036, <https://doi.org/10.1016/j.biortech.2006.10.013> (2007).
- Liu, Q., Zhong, Z., Wang, S. & Luo, Z. Interactions of biomass components during pyrolysis: A TG-FTIR study. *J. Anal. Appl. Pyrol.* **90**, 213–218, <https://doi.org/10.1016/j.jaap.2010.12.009> (2011).
- Biagini, E., Barontini, F. & Tognotti, L. Gasification of agricultural residues in a demonstrative plant: corn cobs. *Bioresource Technol.* **173**, 110–116, <https://doi.org/10.1016/j.biortech.2014.09.086> (2014).
- Wang, S., Liao, Y., Qian, L., Luo, Z. & Cen, K. Experimental study of the influence of acid wash on cellulose pyrolysis. *J. Fuel. Chem. Techn.* **1**, 35–39, <https://doi.org/10.1007/s11705-007-0007-7> (2006).
- Yang, H., Rong, Y., Chen, H., Dong, H. L. & Zheng, C. Characteristics of hemicellulose, cellulose and lignin pyrolysis. *Fuel*. **86**, 1781–1788, <https://doi.org/10.1016/j.fuel.2006.12.013> (2007).
- Rowe, R. C., Parker, M. D. & Mckillop, A. G. The effect of particle size on the heat of immersion of microcrystalline cellulose. *Int. J. Pharmaceut.* **91**, 247–250, [https://doi.org/10.1016/0378-5173\(93\)90345-G](https://doi.org/10.1016/0378-5173(93)90345-G) (1993).
- Hu, L. *et al.* Catalytic conversion of carbohydrates into 5-hydroxymethylfurfural over cellulose-derived carbonaceous catalyst in ionic liquid. *Bioresource Technol.* **148**, 501–507, <https://doi.org/10.1016/j.biortech.2013.09.016> (2013).
- John, B., Paine, I. I. I., Yezdi, B. P. & John, D. N. Carbohydrate pyrolysis mechanisms from isotopic labeling: part 4. the pyrolysis of d-glucose: the formation of furans. *J. Anal. Appl. Pyrol.* **83**, 37–63, <https://doi.org/10.1016/j.jaap.2008.05.008> (2008).
- Wang, H. *et al.* Am1 kinetics research of the pyrolysis mechanism of toluene. *Acta Chim. Sin.* **17**, 545–550, <https://doi.org/10.3321/j.issn:1001-4861.2001.04.014> (2001).
- Wang, H. J., Fu, Y., Liu, L. & Guo, Q. X. Density functional theory study on homolytic bond dissociation enthalpies of carbon-fluorine bond. *Acta Chimica Sinica*. **6**, 033116, <https://doi.org/10.1063/1.4880213> (2007).
- Huang, J., Liu, C., Wei, S. & Huang, X. Density functional theory study on the dehydration mechanism of glycerine. *Acta Chimica Sinica* **68**, 1043–1049, <https://doi.org/10.1631/jzus.B1000073> (2010).
- Payal, R. S., Bharath, R., Periyasamy, G. & Balasubramanian, S. Density functional theory investigations on the structure and dissolution mechanisms for cellobiose and xylan in an ionic liquid: gas phase and cluster calculations. *J. Phys. Chem. B* **116**, 833–840, <https://doi.org/10.1021/jp207989w> (2012).
- Wang, H., Yang, H., Ran, X., Wen, Z. & Shi, Q. The pyrolysis mechanism of carbon matrix precursor toluene used as carbon material. *Theochem* **581**, 1–9, [https://doi.org/10.1016/s0166-1280\(01\)00726-6](https://doi.org/10.1016/s0166-1280(01)00726-6) (2002).

28. Hugo, M., Encina, A., Jesús, Á., José, L. A. & David, C. R. Unraveling the biochemical and molecular networks involved in maize cell habituation to the cellulose biosynthesis inhibitor dichlobenil. *Mol. Plant* **3**, 842–853, <https://doi.org/10.1093/mp/ssp027> (2010).
29. Qiang, L. *et al.* Catalytic pyrolysis of cellulose with sulfated metal oxides: a promising method for obtaining high yield of light furan compounds. *Bioresource. Technol.* **100**, 4871–4876, <https://doi.org/10.1016/j.biortech.2009.04.068> (2009).
30. Qing, Q., Yang, B. & Wyman, C. E. Xylooligomers are strong inhibitors of cellulose hydrolysis by enzymes. *Bioresource. Technol.* **101**, 9624–9630, <https://doi.org/10.1016/j.biortech.2010.06.137> (2010).
31. Geng, Z., Zhang, M. & Yu, Y. Theoretical investigation on pyrolysis mechanism of glycerol. *Fuel*. **93**, 92–98, <https://doi.org/10.1016/j.fuel.2011.08.021> (2012).
32. Zhang, X., Yang, W. & Dong, C. Levoglucosan formation mechanisms during cellulose pyrolysis[J]. *Journal of Analytical and Applied Pyrolysis*. **104**, 19–27, <https://doi.org/10.1016/j.jaap.2013.09.015> (2013).
33. Zhang, Y., Liu, C. & Chen, X. Unveiling the initial pyrolytic mechanisms of cellulose by DFT study. *J. Anal. Appl. Pyrol.* **113**, 621–629, <https://doi.org/10.1016/j.jaap.2015.04.010> (2015).
34. Lu, Q. *et al.* Mechanism of cellulose fast pyrolysis: The role of characteristic chain ends and dehydrated units. *Combust. Flame*. **198**, 267–277, <https://doi.org/10.1016/j.combustflame.2018.09.025> (2018).
35. Hosoya, T., Nakao, Y., Sato, H., Kawamoto, H. & Sakaki, S. Thermal degradation of methyl beta-d-glucoside. a theoretical study of plausible reaction mechanisms. *J. Org. Chem.* **74**, 6891–6894, <https://doi.org/10.1021/jo900457k> (2009).
36. Huang, J., Liu, C., Wu, D., Tong, H. & Ren, L. Density functional theory studies on pyrolysis mechanism of β -O-4 type lignin dimer model compound. *J. Anal. Appl. Pyrol.* **109**, 98–108, <https://doi.org/10.1016/j.jaap.2014.07.007> (2014).
37. Climent, M. J., Corma, A. & Iborra, S. ChemInform Abstract: Converting Carbohydrates to Bulk Chemicals and Fine Chemicals over Heterogeneous Catalysts. *Cheminform.* **13**, 520–540, <https://doi.org/10.1039/C0GC00639D> (2011).
38. Strati, G. L., Willett, J. L. & Momany, F. A. A DFT/ab initio study of hydrogen bonding and conformational preference in model cellobiose analogs using B3LYP/6-311++G*. *Carbohydr. Res.* **337**, 1851–1859, [https://doi.org/10.1016/S0008-6215\(02\)00269-0](https://doi.org/10.1016/S0008-6215(02)00269-0) (2002).
39. Assary, R. S. & Curtiss, L. A. Comparison of sugar molecule decomposition through glucose and fructose: a high-level quantum chemical study. *Energ. Fuel* **26**, 1344–1352, <https://doi.org/10.1021/ef201654s> (2012).
40. Assary, R. S. & Curtiss, L. A. Thermochemistry and Reaction Barriers for the Formation of Levoglucosenone from Cellobiose. *Chemcatchem.* **4**, 200–205, <https://doi.org/10.1002/cctc.201100280> (2011).
41. Kabayemela, B. M., Takigawa, M., Adschiri, T., Malaluan, R. M. & Arai, K. Mechanism and Kinetics of Cellobiose Decomposition in Sub- and Supercritical Water. *Ind. Eng. Chem. Res.* **37**, 357–361, <https://doi.org/10.1021/ie9704408> (1998).
42. Brown, A. L., Dayton, D. C. & Daily, J. W. A Study of Cellulose Pyrolysis Chemistry and Global Kinetics at High Heating Rates. *Energ. Fuel*. **15**, 1286–1294, <https://doi.org/10.1021/ef010084c> (2001).
43. Qiang, L., Li, W. Z., Dong, Z. & Zhu, X. F. Analytical pyrolysis-gas chromatography/mass spectrometry (py-gc/ms) of sawdust with al/sba-15 catalysts. *J. Anal. Appl. Pyrol.* **8**, 131–138, <https://doi.org/10.1016/j.jaap.2009.01.002> (2009).
44. Wang, S., Guo, X., Liang, T., Zhou, Y. & Luo, Z. Mechanism research on cellulose pyrolysis by py-gc/ms and subsequent density functional theory studies. *Bioresource. Technol.* **104**, 722–728, <https://doi.org/10.1016/j.biortech.2017.06.018> (2012).
45. Arseneau, D. F. Competitive reactions in the thermal decomposition of cellulose. *Can. J. Chem.* **49**, 632–638, <https://doi.org/10.1139/v71-101> (1971).
46. Milosavljevic, I., Vahur Oja, A. & Suuberg, E. M. Thermal effects in cellulose pyrolysis: relationship to char formation processes. *Ind. Eng. Chem. Res.* **35**, 653–662, <https://doi.org/10.1021/ie950438l> (1996).
47. Branca, C., Paola Giudicianni, A. & Blasi, C. D. GC/MS Characterization of Liquids Generated from Low-Temperature Pyrolysis of Wood. *Ind. Eng. Chem. Res.* **42**, 3190–3202, <https://doi.org/10.1021/ie030066d> (2003).
48. Thangalazhy-Gopakumar, S. *et al.* Physicochemical properties of bio-oil produced at various temperatures from pine wood using an auger reactor. *Bioresource. Technol.* **101**, 8389–8395, <https://doi.org/10.1016/j.biortech.2010.05.040> (2010).
49. Luo, Z. Y. *et al.* Research on biomass fast pyrolysis for liquid fuel. *Biomass. Bioenerg.* **26**, 455–462, <https://doi.org/10.1016/j.biombioe.2003.04.001> (2004).
50. Luo, Z., Wang, S., Liao, Y. & Cen, K. Mechanism study of cellulose rapid pyrolysis. *Ind. Eng. Chem. Res.* **43**, 5605–5610, <https://doi.org/10.1021/ie030774z> (2004).
51. Piskorz, J., Radlein, D. & Scott, D. S. On the mechanism of the rapid pyrolysis of cellulose. *J. Anal. Appl. Pyrol.* **9**, 121–137, <https://doi.org/10.1021/ie030774z> (1986).
52. Birot, M. *et al.* Investigation of the pyrolysis mechanisms of cellobiose in the presence of a polysiloxane. *J. Anal. Appl. Pyrol.* **81**, 263–271, <https://doi.org/10.1016/j.jaap.2007.12.004> (2008).
53. Sanders, E. B., Goldsmith, A. I. & Seeman, J. I. A model that distinguishes the pyrolysis of d-glucose, d-fructose, and sucrose from that of cellulose. application to the understanding of cigarette smoke formation. *J. Anal. Appl. Pyrol.* **66**, 29–50, [https://doi.org/10.1016/S0165-2370\(02\)00104-3](https://doi.org/10.1016/S0165-2370(02)00104-3) (2003).
54. Huang, J., Liu, C., Wu, D., Tong, H. & Ren, L. Density functional theory studies on pyrolysis mechanism of β -d -glucopyranose. *J. Mol. Struct.-Theochem.* **958**, 64–70, <https://doi.org/10.1016/j.theochem.2010.07.030> (2010).
55. Assary, R. S. & Curtiss, L. A. Thermochemistry and Reaction Barriers for the Formation of Levoglucosenone from Cellobiose. *ChemCatChem.* **4**, 137–137, <https://doi.org/10.1002/cctc.201100280> (2012).
56. Zhang, X., Li, J., Yang, W. & Wlodzimierz, B. Formation Mechanism of Levoglucosan and Formaldehyde during Cellulose Pyrolysis. *Energ. Fuel*. **25**(8), 3739–3746, <https://doi.org/10.1021/ef2005139> (2011).
57. Nimlos, M. R., Blanksby, S. J., Qian, X., Himmel, M. E. & Johnson, D. K. Mechanisms of glycerol dehydration. *J. Phys. Chem. A*. **110**, 6145–6156, <https://doi.org/10.1021/jp060597q> (2006).
58. Taherzadeh, M. J. & Karimi, K. Pretreatment of Lignocellulosic Wastes to Improve Ethanol and Biogas Production: A Review. *Int. J. Mol. Sci.* **9**, 1621–1651, <https://doi.org/10.1016/j.wasman.2012.01.016> (2008).
59. Paine, J. B., Pithawalla, Y. B. & Naworal, J. D. Carbohydrate pyrolysis mechanisms from isotopic labeling part 1: the pyrolysis of glycerin: discovery of competing fragmentation mechanisms affording acetaldehyde and formaldehyde and the implications for carbohydrate pyrolysis. *J. Anal. Appl. Pyrol.* **80**, 297–311, <https://doi.org/10.1016/j.jaap.2018.12.010> (2007).
60. Zhang, M., Geng, Z. & Yu, Y. Density functional theory (DFT) study on the dehydration of cellulose. *Energ. Fuel*. **25**, 2664–2670, <https://doi.org/10.1021/ef101619e> (2011).
61. Nimlos, M. R., Blanksby, S. J. & Ellison, G. B. Enhancement of 1,2-dehydration of alcohols by alkali cations and protons: a model for dehydration of carbohydrates. *J. Anal. Appl. Pyrol.* **66**, 3–27, [https://doi.org/10.1016/S0165-2370\(02\)00103-1](https://doi.org/10.1016/S0165-2370(02)00103-1) (2003).
62. Banyasz, J. L., Li, S., Lyons-Hart, J. L. & Shafer, K. H. Cellulose pyrolysis: the kinetics of hydroxyacetaldehyde evolution. *J. Anal. Appl. Pyrol.* **57**, 223–248, [https://doi.org/10.1016/S0165-2370\(00\)00135-2](https://doi.org/10.1016/S0165-2370(00)00135-2) (2001).
63. Lu, Q., Tian, H. Y. N. & Hu, B. Pyrolysis mechanism of holocellulose-based monosaccharides: The formation of hydroxyacetaldehyde. *J. Anal. Appl. Pyrol.* **2016**(120), 15–26, <https://doi.org/10.1016/j.jaap.2016.04.003> (2016).
64. Choudhary, V., Burnett, R. I., Vlachos, D. G. & Sandler, S. I. Dehydration of glucose to 5-(hydroxymethyl) furfural and hydroglucose: thermodynamic insights. *J. Phys. Chem. C*. **116**, 5116–5120, <https://doi.org/10.1021/jp2113895> (2013).
65. Agirrezabaltegeria, I., Gandarias, I. & Arias, P. L. Heterogeneous acid-catalysts for the production of furan-derived compounds (furfural and hydroxymethylfurfural) from renewable carbohydrates: A review. *Catal. Today*. **234**, 42–58, <https://doi.org/10.1016/j.cattod.2013.11.027> (2014).

66. Vinu, R. & Broadbelt, L. J. A mechanistic model of fast pyrolysis of glucose-based carbohydrates to predict bio-oil composition. *Energ Environ Sci.* **5**, 9808, <https://doi.org/10.1039/c2ee22784c> (2012).
67. Liu, Q., Zhong, Z., Wang, S. & Luo, Z. 2011. Interactions of biomass components during pyrolysis: a TG-FTIR study. *J. Anal. Appl. Pyrol.* **90**, 213–218, <https://doi.org/10.1016/j.jaap.2010.12.009> (2010).
68. Zhang, Y. Y., Liu, C. & Xie, H. Mechanism studies on β -d-glucopyranose pyrolysis by density functional theory methods. *J. Anal. Appl. Pyrolysis.* **105**, 23–34, <https://doi.org/10.1016/j.jaap.2013.09.016> (2013).

Acknowledgements

The authors appreciate financial support granted from the National Key R&D Program of China (NO. 2018YFB1501405).

Author contributions

Wang Q. conceived the experiment(s), Song H. and Wang Q. conducted the experiment(s), Wang Q., Pan S. and Dong N.H. analysed the results. Song H., Wang X.M. and Sun S.P. verified the model. All authors reviewed the manuscript.

Competing interests

The authors declare no competing interests.

Additional information

Supplementary information is available for this paper at <https://doi.org/10.1038/s41598-020-60095-2>.

Correspondence and requests for materials should be addressed to Q.W.

Reprints and permissions information is available at www.nature.com/reprints.

Publisher's note Springer Nature remains neutral with regard to jurisdictional claims in published maps and institutional affiliations.



Open Access This article is licensed under a Creative Commons Attribution 4.0 International License, which permits use, sharing, adaptation, distribution and reproduction in any medium or format, as long as you give appropriate credit to the original author(s) and the source, provide a link to the Creative Commons license, and indicate if changes were made. The images or other third party material in this article are included in the article's Creative Commons license, unless indicated otherwise in a credit line to the material. If material is not included in the article's Creative Commons license and your intended use is not permitted by statutory regulation or exceeds the permitted use, you will need to obtain permission directly from the copyright holder. To view a copy of this license, visit <http://creativecommons.org/licenses/by/4.0/>.

© The Author(s) 2020